PAPER

Optical transitions and radiative properties of green emitting Ho³⁺:YVO₄ phosphor

Vijay Singh, [ID] *[a] M. Seshadri,[b] Deepak Taikar,[c] S. J. Dhoble[d] and R. S. Yadav [ID] [e]

The Ho³⁺-doped YVO₄ phosphors were successfully prepared _via_ a sol–gel process in which citric acid was used as a chelating agent. X-ray diffraction (XRD) confirmed the effective inclusion of Ho³⁺ ions into the host matrix with the formation of single phase YVO₄. The surface morphology was observed using SEM, the results of which showed a grain growth propensity and the agglomeration of prepared phosphors. The V–O (VO₄³⁻) vibration mode was analyzed through Fourier transform infrared (FTIR) spectra. The spectroscopic properties were reported through UV-vis-NIR diffuse reflectance and photoluminescence (PL) spectra. The Judd–Ofelt (J–O) intensity parameters $\Omega_2 = 0.03 \times 10^{-20}$ cm², $\Omega_4 = 0.22 \times 10^{-20}$ cm², and $\Omega_6 = 0.23 \times 10^{-20}$ cm² obtained for the $Y_{0.97}VO_4:0.03Ho^{3+}$ phosphors were used to obtain the total transition probabilities (A_T), radiative lifetimes (τ_{rad}) and branching ratios (β) for the certain transitions of Ho³⁺ ions. Under 310 nm UV excitation, the visible emission spectra were measured, and an intense emission was observed around 541 nm (green region) for all the samples. The emission cross-section $\sigma_P(\lambda)$ was 3.22×10^{-21} cm² and the branching ratio (β) was 0.816; these were investigated to capture the optimal concentration of the $Y_{0.97}VO_4:0.03Ho^{3+}$ phosphor. The estimated color coordinates were observed in the green region of CIE diagram. Ultimately, the superior properties ($\sigma_P(\lambda)$, β, and color purity) of $Y_{0.97}VO_4:0.03Ho^{3+}$ phosphor may make it suitable for green emitting devices.

1. Introduction

Recently, the zircon structured orthovanadate (AVO₄, A = trivalent metal ion) has attracted substantial research attention because of its applicability in a wide variety of areas.[1] This material is not only used as a luminescent host material but has also been used in diverse applications in the fields of gas sensing, high power lasers, fuel cell anodes, and counter electrodes in electrochromic devices.[2–4] Yttrium vanadate (YVO₄) is a well-recognized host lattice for rare-earth (RE) activators from the family of AVO₄. YVO₄ shows excellent thermal, mechanical, and optical properties, and it exhibits wide absorption in the UV region; therefore, RE doped phosphors are widely used for optoelectronic application alongwith biosensors and laser devices.[5–12] YVO₄ shows high birefringence and can be used as a polarizer in the infrared (IR) region.[13] YVO₄ is also a good up-conversion host due to its low phonon energy (~880 cm⁻¹). Many studies have examined up-conversion luminescence in RE³⁺-doped and co-doped YVO₄ phosphors.[14–17] YVO₄:Nd³⁺

performs better than YAG:Nd³⁺, and it is therefore a good laser excitable host crystal for Nd³⁺ ions, and has shown remarkable applicability in laser-diode pumped micro lasers.[18–21]

At present, to conquer multiple color tunability, the phosphor materials are used in energy conversion and materials technology. Due to its efficient energy conversion, the high color purity and thermal stability of Eu³⁺-doped YVO₄ make it a promising red phosphor for use in a wide range of applications in luminescence and display devices, such as fluorescent lamps, cathode ray tubes, plasma display panels, _etc._[22–30] Foka _et al._[31] synthesized Dy³⁺-doped YVO₄ phosphor _via_ the combustion route and reported white emission with excitation in the UV region. Liu _et al._[32] synthesized YVO₄:Ln³⁺ (Ln = Eu, Sm, Dy) _via_ the microwave heating method and reported its morphology and photoluminescence (PL) results. Xu _et al._[33] studied the effects of organic additives on the shape and morphology of RE³⁺-doped YVO₄ phosphors synthesized _via_ a hydrothermal method. They have found remarkable results, which can be used for tunability in the display panels. Their PL study indicates an efficient multicolor emission that can be useful in lasers and displays related to the optoelectronic devices. Huang _et al._[34] synthesized (Bi³⁺, RE³⁺) co-doped YVO₄ phosphor by a solid-state reaction technique and reported that the phosphors could improve the efficiency of the power conversion of dye-sensitized and crystalline silicon (c-Si) solar cells. The energy transfer between single and triply doped RE³⁺ ions in the YVO₄ host and its luminescence property have

ᵃDepartment of Chemical Engineering, Konkuk University, Seoul, 05029, Republic of Korea. E-mail: vijayjiin2006@yahoo.com

ᵇDepartment of Physics, KG Reddy College of Engineering and Technology, Hyderabad-501504, India

ᶜDepartment of Physics, Shri Lemdeo Patil Mahavidyalaya, Mandhal, 441210, India

ᵈDepartment of Physics, R.T.M. Nagpur University, Nagpur, 440033, India

ᵉDepartment of Zoology, Institute of Science, Banaras Hindu University, Varanasi, 221005, India

recently been studied by Medvedev *et al.*[35] Moreover, all the rare earth ions and their doped systems of the phosphors with Ho³⁺ ion serve as good activators due to energy transfer and reflecting the multiple color emission. Zhou *et al.*[36] studied the PL property of red emitting YVO₄:Pr³⁺ phosphor, which is considered to be a good candidate for optical thermal sensing applications. YVO₄ phosphors have been synthesized through various synthesis methods, such as co-precipitation,[37] solution combustion,[38] solid state reaction,[34] microwave heating,[32] sol–gel,[39,40] microemulsions,[41] solvothermal,[42] ultrasonic,[43] and spray pyrolysis methods.[44] The YVO₄:(Ho³⁺,Yb³⁺) phosphors synthesized by different synthesis method and their effect on luminescence have recently been studied.[39] The study indicates that the YVO₄:(Ho³⁺,Yb³⁺) phosphor prepared by sol–gel method exhibit better optical properties than the phosphor synthesized by the combustion and solid state reaction methods.

In the present work, most notably, we have successfully synthesized trivalent holmium (Ho³⁺)-doped YVO₄ phosphors with different doping concentrations. The samples were characterized in terms of their physical and radiative properties by using X-ray diffraction (XRD), scanning electron microscopy (SEM), Fourier transform infrared (FTIR) spectroscopy, ultraviolet-visible (UV-vis) spectrometry, and photoluminescence (PL) techniques.

2. Materials preparation and analysis

Phosphor materials of $Y_{1-x}VO_4$:xHo³⁺ ($x = 0.01, 0.03, 0.05, 0.07, 0.09, 0.11$) were prepared through the sol–gel method. The details of the sample composition and the starting materials along with required weights are given in Table 1. The appropriate amounts of Y(NO₃)₃·6H₂O, NH₄VO₃, Ho(NO₃)₃·5H₂O, and citric acid (chelating agent for the metal ions) were weighed and added into a 150 ml glass beaker with 10 ml deionized water. The prepared solution was stirred for 1 hour to ensure uniform homogeneity. Next, the solution was placed in a hot oven until it was completely dried. The dried gels were heated in air at 400 °C for upto 2 hours. The preheated powder samples were ground and again heated in air at 800 °C for 2 hours to acquire the final samples. Fig. 1 shows a flow chart of the synthesis method.

The phase of prepared powders was identified using a RIGAKU (Miniflex-II) XRD spectrometer with CuKα light radiation as X-ray. FTIR spectrum in the 4000–400 cm⁻¹ range was obtained on a Thermo Fisher Nicolet (6700 FT-IR)

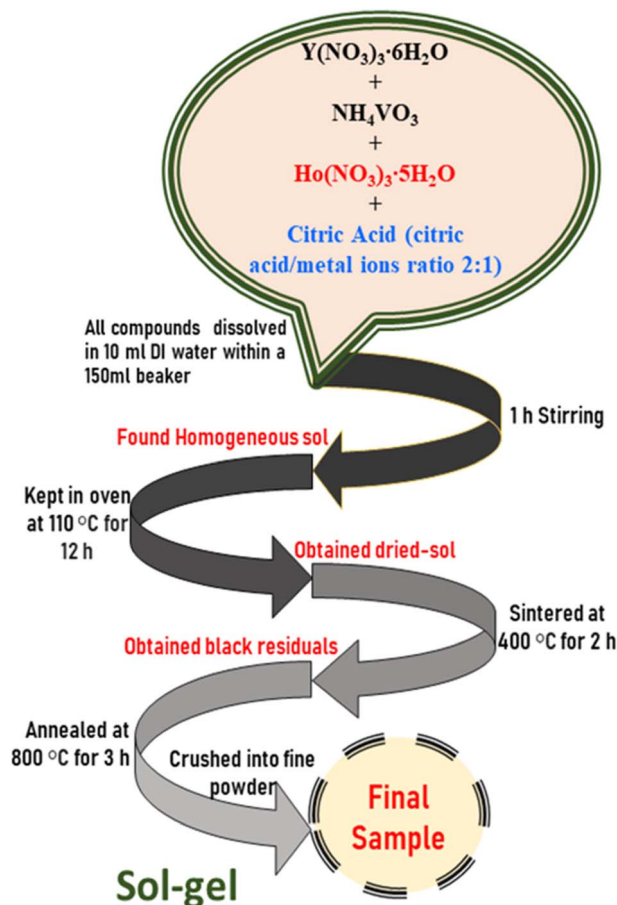**Fig. 1** Flow chart of synthesis method of $Y_{1-x}VO_4$:xHo³⁺ phosphors.

spectrometer utilizing KBr pellets. The sample surface morphology was imaged using a S-3400, SEM (Hitachi, Japan). The diffuse reflection spectrum was captured with a UV-VIS-NIR (Cary-5000) spectrophotometer. PL characterizations were carried out at room temperature using a RF-5301PC, Shimadzu, fluorescence spectrophotometer with a Xenon flash lamp as an excitation source.

3. Results and discussion

Fig. 2 shows the crystal structure of the YVO₄ compound with different orientations. YVO₄ is (zircon type structure) crystallized in the tetragonal $I4_1$/amd space group. In this structure,

Table 1 Detailed information of sample and weight of the required starting materials

Samples	Base materials			
$Y_{0.99}VO_4$:0.01Ho³⁺	$Y = 0.7583$g	$V = 0.2338$g	C.$A = 1.5368$g	Ho = 0.0176g
$Y_{0.97}VO_4$:0.03Ho³⁺	$Y = 0.7430$g	$V = 0.2338$g	C.$A = 1.5368$g	Ho = 0.0592g
$Y_{0.95}VO_4$:0.05Ho³⁺	$Y = 0.7277$g	$V = 0.2338$g	C.$A = 1.5368$g	Ho = 0.0882g
$Y_{0.93}VO_4$:0.07Ho³⁺	$Y = 0.7123$g	$V = 0.2338$g	C.$A = 1.5368$g	Ho = 0.1243g
$Y_{0.91}VO_4$:0.09Ho³⁺	$Y = 0.6970$g	$V = 0.2338$g	C.$A = 1.5368$g	Ho = 0.1578g
$Y_{0.89}VO_4$:0.11Ho³⁺	$Y = 0.6817$g	$V = 0.2338$g	C.$A = 1.5368$g	Ho = 0.1940g

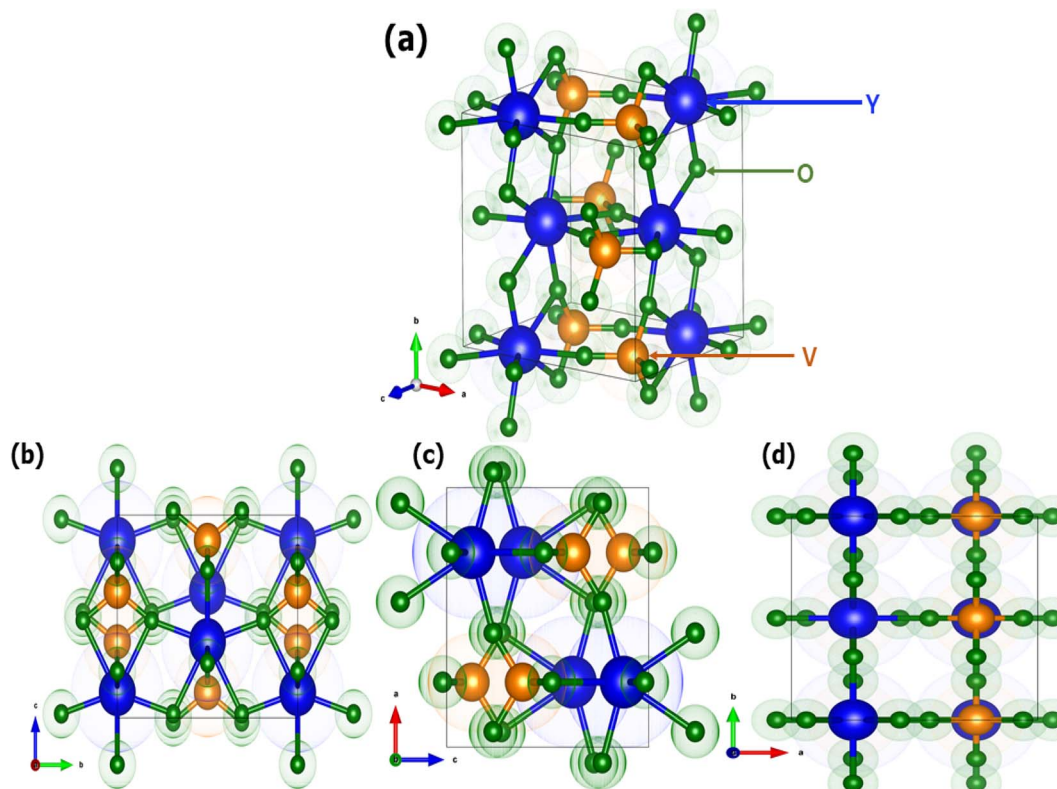Y = Y(NO₃)₃·6H₂O, V = NH₄VO₃, C.A = citric acid, Ho = Ho(NO₃)₃·5H₂O

Fig. 2 Crystal structure of YVO$_4$ (a) standard orientation and (b–d) three different orientations 100, 010, and 001.

Y^{3+} atom has D_{2d} site symmetry and is bonded in 8-coordinate geometry to eight equivalent O^{2-} atoms to form an anti-prism. Out of these eight Y–O bonds, four have shorter bond lengths (2.33 Å) whereas the other four have longer bond lengths (2.45 Å). The V^{5+} atom is bonded with four equivalent O^{2-} atoms to form VO$_4^{3-}$ tetrahedra which share edges with YO$_8$ dodecahedrons, as shown in Fig. 2. All V–O bond lengths are 1.74 Å. The

O^{2-} atom is bonded with two equivalent Y^{3+} atoms and one V^{5+} atom.[45,46] Fig. 3 shows the observed XRD patterns of the YVO$_4$ phosphors produced through the sol–gel technique. The observed XRD patterns are counterpart with the standard card of JCPDF 70-1281. No miscellaneous or additional peak is observed in all the XRD patterns, thus suggesting a single-phase material and indicates that the crystal structure of host matrix does not change with the addition of Ho^{3+} ion. The ionic radius of Ho^{3+} ($r = 0.89$ Å) was found to be well matched with ionic radius of Y^{3+} ($r = 0.9$ Å, CN = 8), thus indicates that the Ho^{3+} is successfully incorporated at the Y^{3+} sites. The XRD pattern shows that the prepared YVO$_4$ crystallizes in the tetragonal $I4_1/amd$ space group alongwith cell parameters $a = 7.120$ Å, $c = 6.289$ Å, and volume = 318.82 Å^3. The average crystallite size can be determined using the formula,

$$D = 0.9\lambda/\beta \cos\theta \qquad (1)$$

here, λ (1.540598 Å) is the wavelength of X-ray radiation, and the diffraction angle of Bragg's (θ) and Full width at half maxima (FWHM) is denoted by β. The average crystallite size of the phosphor samples was within the 20–30 nm range.

Fig. 4 presents SEM images of the synthesized Y$_{0.97}$VO$_4$:0.03Ho^{3+} phosphor. The inhomogeneous morphology and large grain size are observed in the SEM images. SEM images reveal that the phosphor particles morphologies are not uniform, they also show that the phosphor particles are irregular and agglomerated Fig. 4(b) shows an enlarged view of the
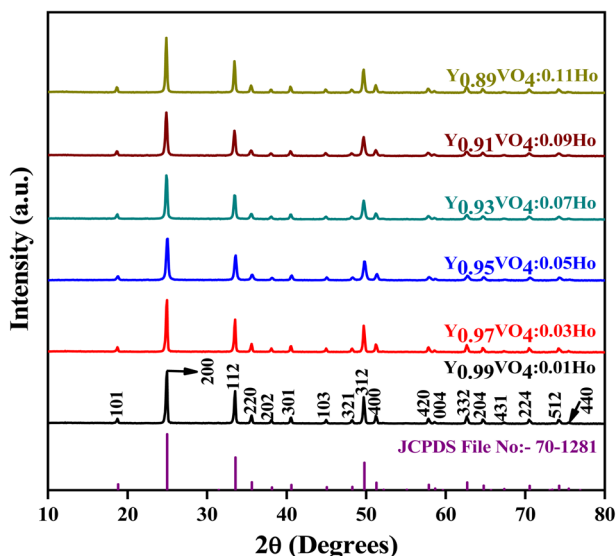

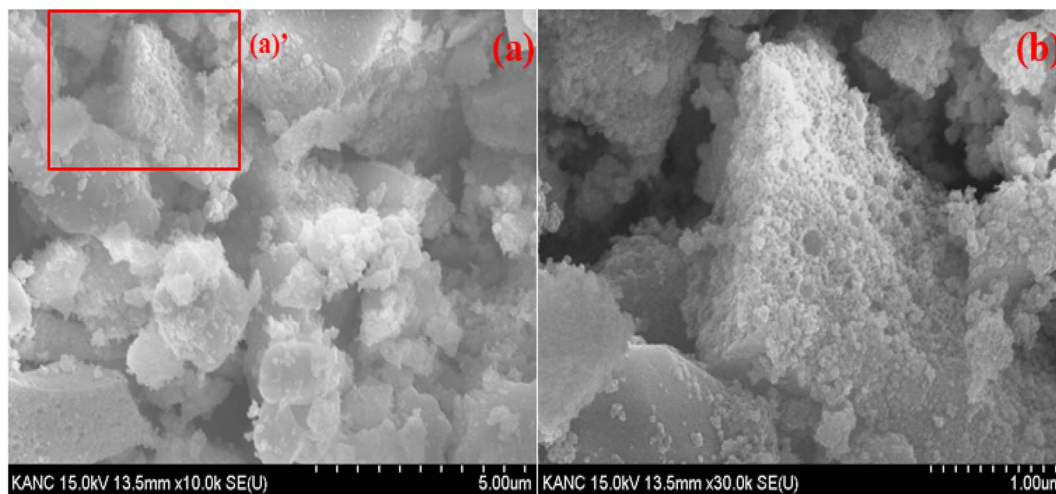**Fig. 3** Powder XRD patterns of Y$_{1-x}$VO$_4$:xHo^{3+} phosphors.

Fig. 4 (a) SEM image of $Y_{0.97}VO_4{:}0.03Ho^{3+}$ phosphor and (b) enlarged view of zone (a)′.

"zone (a)′" of Fig. 4(a), wherein the sample consists of voids, and pores that are most likely due to the evolution of large amount of gases during the process of sintering. The grain size distribution is broad, and the average particles size ranges from 100 nm to 500 nm for the $Y_{0.97}VO_4{:}0.03Ho^{3+}$ phosphor. These characteristics suggest that the optical properties are suitable for the industrial use.

Fig. 5 reveals the FTIR spectrum of $Y_{0.97}VO_4{:}0.03Ho^{3+}$ phosphor, which is used to analyze the chemical structure and presence of the functional groups associated with the crystal. The intense band situated at 814 cm^{-1} is remarkably matched with the characteristic vibrational modes of the V–O group of the tetrahedral structure of $VO_4{}^{3-}$ group.[47] The weak band occurring at 450 cm^{-1} is attributable to the Y–O group of structural vibrations. The very weak bands observed between 1100 to 1400 cm^{-1} is due to the presence of C–O and nitrate groups alongwith the band between 1400 to 1500 cm^{-1}
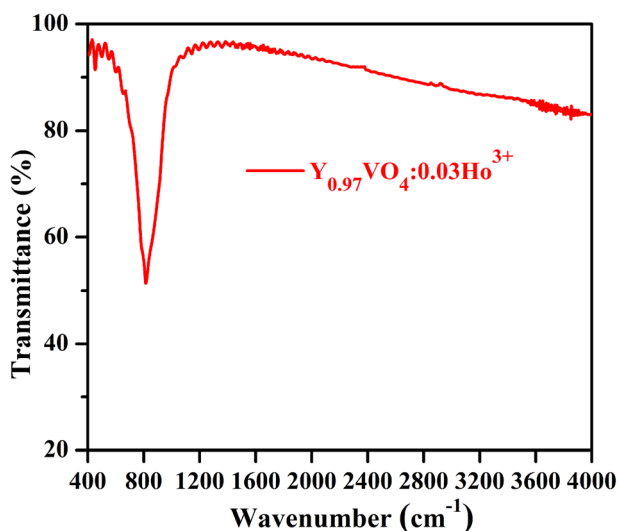
associated with the vibrations of carboxylate anions of the citric acid. A very weak band observed at 2350 cm^{-1} corresponds to the asymmetrical stretching modes of CO_2.[17] Some very weak bands beyond 3500 cm^{-1} are also assigned to the water molecules present on the sample surface.

Fig. 6(a) depicts the diffuse reflectance spectrum of $Y_{0.97}VO_4{:}0.03Ho^{3+}$ phosphor. The sharp peaks observed around 421, 458, 469, 478, 489, 544, and 651 nm are associated with the transitions from the ground state of $^5I_8$ to the $^5G_5$, $^5G_6 + {}^5F_1$, $^3K_8$, $^5F_2$, $^5F_3$, $^5F_4 + {}^5S_2$, and $^5F_5$ excited states of Ho^{3+} ions, respectively.[48,49] The extracted absorption coefficient (α cm^{-1}) with the Kubelka–Munk function can be written as:[48]

$$F(R) = \frac{(1-R)^2}{2R} = \alpha \qquad (2)$$

where R is the sample reflectance. The extracted optical coefficient (α cm^{-1}) can be calculated by using relation (2). The optical band gap (E_g) for the $Y_{0.97}VO_4{:}0.03Ho^{3+}$ phosphor can be estimated using the Tauc relation:[48]

$$F(R)\, hv \approx A(hv - E_g)^n \qquad (3)$$

where A is a constant, $F(R)$ is the absorption coefficient, hv is the energy of the photon, and $n = 1/2$ (and/or 2) for allowed direct (and/or indirect) transition. Fig. 6(b and c) represents the variation between the $(F(R){*}hv)^n$ and hv (eV). By generalizing the linear region of the plot to $(F(R){*}hv)^2 = 0$ and $(F(R){*}hv)^{1/2} = 0$, the energy bandgaps for the indirect and direct allowed transitions are found to be 3.30 ± 0.24 eV and 3.59 ± 0.38 eV, respectively for the Ho^{3+} doped YVO_4 phosphor.

The Judd–Ofelt theory[49,50] is used to characterize the spectroscopic properties of rare earth doped host matrix, for which details are available elsewhere.[51] Therefore, these remarkable outcomes explain the existence theory of the material properties. The doped YVO_4 phosphor is an excellent host matrix for rare earth doping to support the energy conversion to the Ho^{3+} ions. According to Judd–Ofelt theory, the oscillator strengths
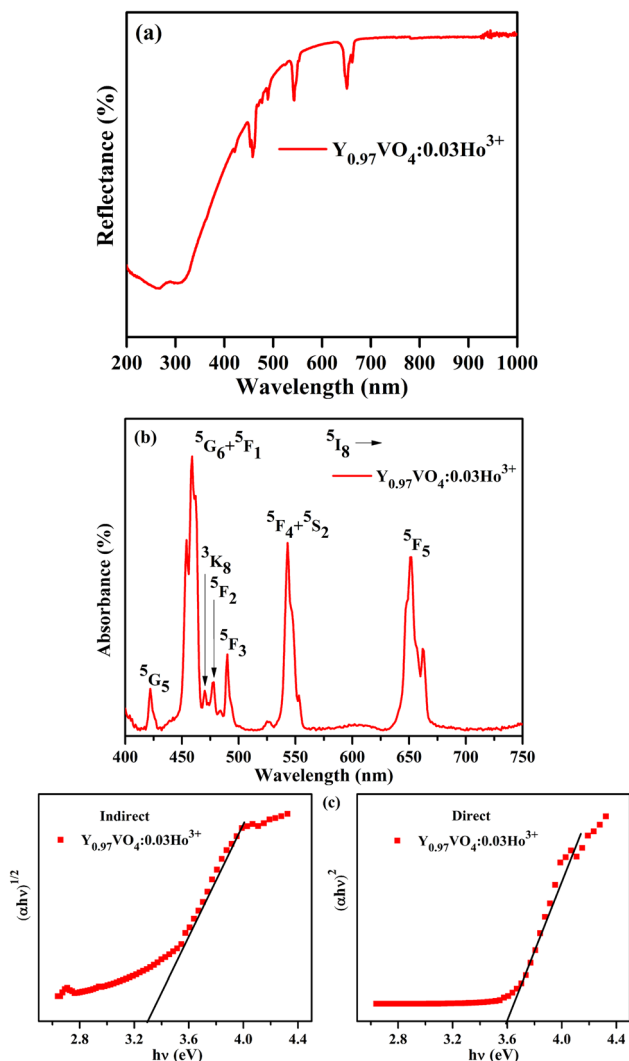

Fig. 5 FT-IR spectrum of $Y_{0.97}VO_4{:}0.03Ho^{3+}$ phosphor.

Fig. 6 (a) Diffuse reflection spectrum, (b) absorption spectrum and (c) plots of indirect and direct bandgaps of $Y_{0.97}VO_4$:0.03Ho^{3+} phosphor.

(f_{cal}) of an electric dipole multiplets $(J \rightarrow J')$ of Ho^{3+} can be expressed as,

$$f_{cal} = \frac{8\pi^2 mc \cdot (n^2+2)^2}{3h(2J+1)\lambda \cdot 9n} \times \sum_{\lambda=2,4,6} \Omega_\lambda |\langle (SL)J \| U^{(\lambda)} \| (S'L')J \rangle|^2 \quad (4)$$

where Ω_λ ($\lambda = 2, 4$ & 6) are the J–O intensity parameters and $U^{(\lambda)}$ are the doubly diminished matrix elements taken from ref. 52, and these tensor operators are independent of the host. The measured oscillator strengths (f_{meas}) for the observed absorption bands are calculated using,[53]

$$f_{meas} = \frac{mc^2}{\pi e^2 \lambda^2 N} \times \frac{2.303}{d} \int OD(\lambda) d\lambda \quad (5)$$

where N is the ion concentration (ions/cm^3), d is the sample thickness, and OD (λ) is the optical density as a function of wavelength. Table 2 reports the oscillator strength $(f_{meas}$ and $f_{cal})$ for Ho^{3+}:YVO$_4$ phosphor alongwith the other hosts. Ω_λ

parameters are evaluated through a standard least square fitting method with the known oscillator strengths of the absorption transitions. The magnitude of root mean square (δ_{rms}) provides information on the quality of the fit, and its formula is,

$$\delta_{rms} = [(f_{meas} - f_{cal})^2/(p-q)]^{1/2} \quad (6)$$

where p and q are the number of transitions employed to the fit and the required fixed parameters, respectively. The observed small r.m.s. deviation (see Table 2) indicates the authenticity of J–O theory.

Table 3 shows the J–O intensity parameters $(\Omega_2, \Omega_4,$ and $\Omega_6)$ of various host matrices. It is well known that the Ω_2 parameter is associated with the covalency of the Ho–O bond, and that the Ω_4 and Ω_6 intensity parameters are related to the bulk properties of the host matrix. From Table 3, it can be seen that the magnitude of Ω_2 in YVO$_4$ phosphor is comparable with that in the YAG (Y$_3$A$_5$O$_{10}$) and lower than those in the other reported host matrices, thus indicates lower covalency around the Ho–O bond. Using the J–O intensity parameter, Ω_λ values; the transition probabilities for the radiative transitions (A_{rad}), excited states of radiative lifetimes (τ_R), and branching ratios (β) are calculated for the Ho^{3+}:YVO$_4$ phosphor using the formula,[53]

$$A_{rad} = \frac{64\pi^4 \nu^3}{3hc^3(2J+1)} \frac{n(n^2+1)^2}{9} \sum_{\lambda=2,4,6} \Omega_\lambda |\langle (SL)J \| U^{(\lambda)} \| ((S'L')J') \rangle|^2 \quad (7)$$

$$t_R = 1/A_T \quad (8)$$

$$\beta = A_{rad}/A_T \quad (9)$$

where A_T is the total radiative transition probability and is estimated by the sum of the A_{rad}. Table 4 represents total radiative transition probabilities (A_T), radiative lifetime (τ_{rad}) of certain excited states, and branching ratios for certain emission transitions of Ho^{3+} ions in YVO$_4$ phosphor. From Table 4, it can be seen that the magnitudes of radiative lifetime for the excited levels are in the order of $^3K_8 > ^5F_5 > ^5F_2 > ^5F_3 > ^5F_4 > ^3H_5 > ^5G_6$. The observed magnitudes of the radiative lifetimes of Ho^{3+}:YVO$_4$ are comparatively higher than those of the reported Ho^{3+} doped hosts: CaScO$_4$,[54] SrLaGaO$_4$,[55] Y$_2$O$_3$,[58] and Lu$_2$SiO$_5$,[60] respectively.

Fig. 7(a) represents the PL excitation spectra of Y$_{1-x}$VO$_4$:xHo^{3+} phosphor materials in the wavelength range from 220 to 530 nm that are obtained by observing the emission wavelength at 541 nm. The broad excitation band appearing between the ~220 and 350 nm wavelength range is the charge transfer (CT) transition (at 310 nm) from the oxygen ligand (O^{2-}) to the central vanadium atom (V^{5+}) within the VO$_4^{3-}$ group, as well as the CT band (at 270 nm) from O^{2-} to Ho^{3+} ions.[32,44,61,62] Some sharp excitation peaks appear at ~360, 420, 450, 456, 468, 475, and 487 nm, and these are attributed to the transitions from the ground state $^5I_8$ to $^3H_6$, $^5G_5$, $^5F_1$,$^5G_6$, $^3K_8$, $^5F_2$, and $^5F_3$ of the excited states of Ho^{3+} ions, respectively.[63] Among all these observed sharp peaks, the 456 nm peak is the most prominent.

Table 2 Measured and calculated oscillator strengths (f_{exp} and f_{cal}) for Ho^{3+} ions in the $Y_{0.97}VO_4:0.03Ho^{3+}$ phosphor

[S'L'J'] manifold	λ (nm)	$Y_{0.97}VO_4:0.03Ho^{3+}$ [a]		$CaSc_2O_4$ (ref. 54)	$SrLaGaO_4$ (ref. 55)	$Y_3Al_5O_{10}$ (ref. 56)
		$f_{meas} \times 10^{-6}$	$f_{cal} \times 10^{-6}$	$f_{meas} \times 10^{-6}$	$f_{meas} \times 10^{-6}$	$f_{meas} \times 10^{-6}$
$^5G_5$	421	0.05	0.35	1.11	—	3.61
$^5G_6 + {}^5F_1$	458	0.73	0.74	5.47	20.7	5.83
$^3K_8$	469	0.01	0.11	—	0.29	4.03
$^5F_2$	478	0.03	0.11	—	0.10	
$^5F_3$	489	0.09	0.20	—	0.92	
$^5S_2 + {}^5F_4$	544	0.48	0.62	1.73	3.86	4.72
$^5F_5$	651	0.68	0.44	2.12	3.37	3.86
δ_{rms}		0.45		0.14	5.36	0.89

[a] Present work.

Table 3 Judd–Ofelt intensity parameters (Ω_λ, $\lambda = 2$, 4 & 6) for Ho^{3+} ions in the host matrices

Host matrix	Ω_2	Ω_4	Ω_6
$Y_{0.97}VO_4:0.03Ho^{3+}$ [a]	0.03	0.22	0.23
$CaSc_2O_4$(ref. 54)	3.78	5.17	1.92
$SrLaGaO_4$(ref. 55)	1.25	0.42	1.80
$Y_3Al_5O_{10}$(ref. 56)	0.04	2.67	1.89
$SrLaGa_3O_7$(ref. 57)	2.23	0.85	1.81
Y_2O_3(ref. 58)	0.45	0.59	0.32
$LiYF_4$(ref. 59)	1.16	2.24	2.09

[a] Present work.

Table 4 Radiative properties of certain excited levels/transitions of Ho^{3+} ions in the $Y_{0.97}VO_4:0.03Ho^{3+}$ phosphor

[S'L'J'] manifold	A_T (s^{-1})	τ_{rad} (μs)
$^3H_5$	1497	668
$^5G_6$	1592	628
$^3K_8$	159	6297
$^5F_2$	867	1153
$^5F_3$	1060	943
$^5F_4$	1082	924
$^5F_5$	542	1845

Transition	β
$^3H_5 \rightarrow {}^5I_8$	0.423
$^5G_6 \rightarrow {}^5I_8$	0.752
$^3K_8 \rightarrow {}^5I_8$	0.880
$^5F_2 \rightarrow {}^5I_8$	0.566
$^5F_3 \rightarrow {}^5I_8$	0.524
$^5F_4 \rightarrow {}^5I_8$	0.816
$^5F_5 \rightarrow {}^5I_8$	0.775

Under UV excitation of 310 nm, the PL emission spectra of $Y_{1-x}VO_4:xHo^{3+}$ phosphors are measured from the 450 nm to 700 nm wavelength region, and the results are represented in Fig. 7(b). The emission spectra show intense green emissions around 541, 546, and 551 nm, which are attributed to the $(^5S_2 + {}^5F_4) \rightarrow {}^5I_8$ transitions of Ho^{3+} ion. A few small emission peaks are observed around 475 nm ($^5F_2 \rightarrow {}^5I_8$), 485 nm ($^5F_3 \rightarrow {}^5I_8$), 526 nm ($^5G_5 \rightarrow {}^5I_7$), and 650 and 661 nm ($^5F_5 \rightarrow {}^5I_8$) wavelengths.[63,64] Fig. 8 shows the energy level diagram of Ho^{3+} ion with possible transitions. Under UV excitation at 310 nm, the excitation energy is first absorbed by VO_4^{3-} group, which excites the electrons from the filled oxygen 2p levels in the valence band to the empty vanadium 3d levels of the conduction band. The emission from the VO_4^{3-} group is not observed in this phosphor. Instead of emission from the VO_4^{3-} group, the resonant energy transfer takes place from the VO_4^{3-} group to the $^5G_4$ level of the Ho^{3+} ion. From $^5G_4$ level, the non-radiative transitions take place to lower lying levels of Ho^{3+} ion and due to this, various emissions take place at different wavelengths as indicated in Fig. 8.

In general, the doping concentration could affect the efficiency or performance of the phosphor, so it is necessary to analyze the effect of Ho^{3+} ion concentration on the PL intensity. In the present analysis, the concentration of Ho^{3+} ion in the YVO_4 host is varied from 0.01 to 0.11 mol, and the resultant PL intensity as a function of Ho^{3+} ion concentration is shown in Fig. 9. The PL intensity is maximum at $x = 0.03$, and it then decreases due to the effect of concentration quenching. This result suggests that the optimum concentration of Ho^{3+} ion in the YVO_4 host is 0.03 mol. The concentration quenching depends on the critical distance (R_C) between the activator ion and the quenching site. According to Blasse, R_C can be calculated using the following expression:[65]

$$R_c = 2\left(\frac{3V}{4\pi X_C N}\right)^{1/3} \quad (10)$$

here, V = volume of unit cell, X_c = optimal concentration of Ho^{3+} ions, and N = number of dopant sites available in the unit cell. In our case, $V = 318.82$ Å^3, $X_c = 0.03$, and $N = 4$. From eqn (10), this equates to a critical distance of 17.18 Å, which is greater than 5 Å, thus indicating a smaller chance of energy transfer via exchange interaction. Therefore, the process of energy transfer occurs via electric multipolar interaction, which causes concentration quenching of Ho^{3+} ion in the prepared phosphors.

The peak stimulated emission cross-section (σ_p) for the $(^5S_2 + {}^5F_4) \rightarrow {}^5I_8$ transition of Ho^{3+} ion for the optimum
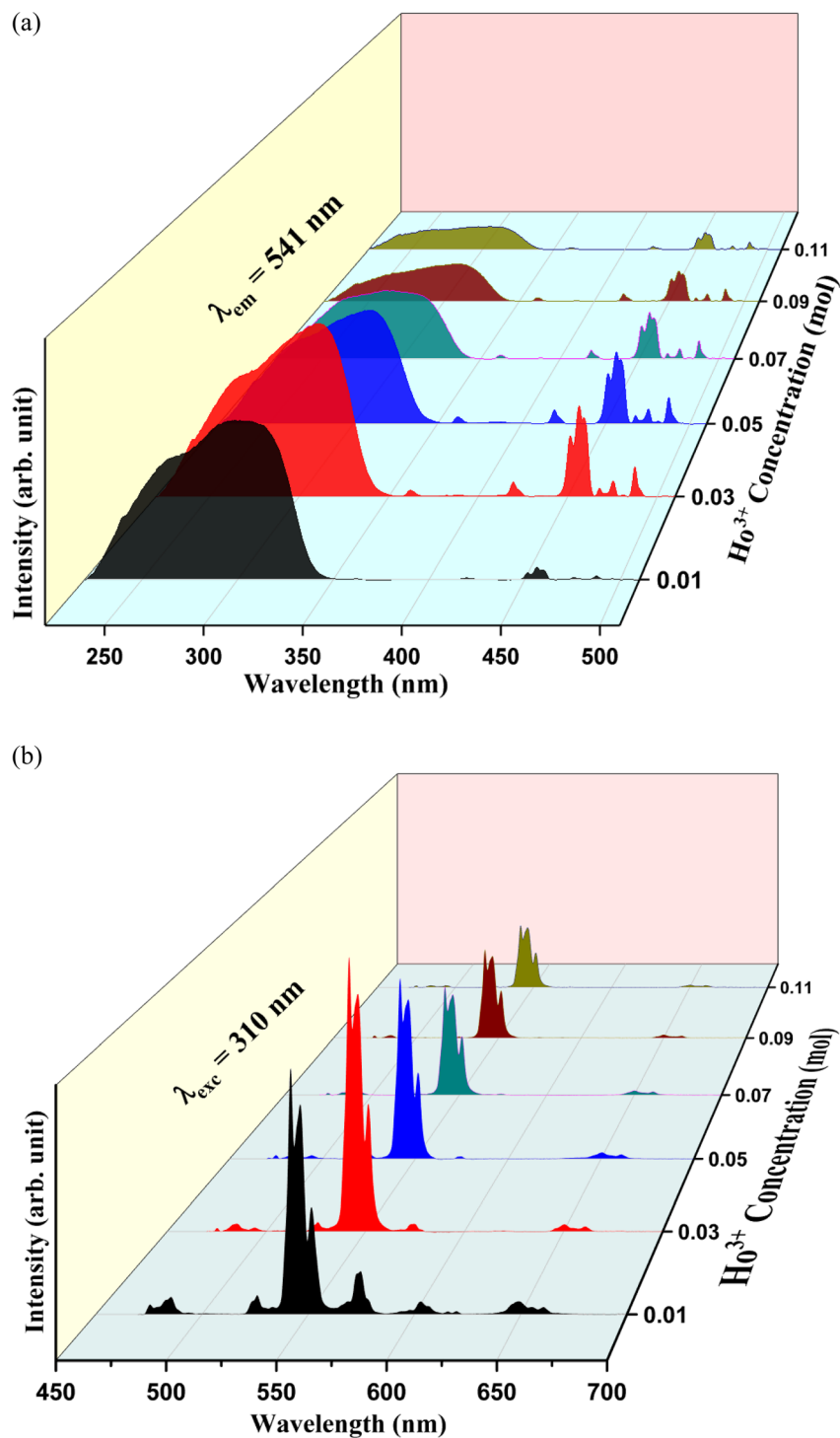
Fig. 7 Photoluminescence spectra of $Y_{1-x}VO_4:xHo^{3+}$ phosphors: (a) excitation spectra ($\lambda_{emi} = 541$ nm) and (b) emission spectra ($\lambda_{exc} = 310$ nm).

$(Y_{0.97}VO_4:0.03Ho^{3+})$ phosphor is also obtained from the following relation[53]

$$\sigma_p(\lambda) = \frac{\lambda_p^4}{8\pi cn^2 \Delta\lambda_{eff}} \cdot A_{rad} \qquad (11)$$

Here, λ_P and $\Delta\lambda_{eff}$ are the peak wavelength and effective line width of the emission band, respectively. The estimated $\Delta\lambda_{eff}$ and $\sigma_p(\lambda)$ are 6.33 nm and 3.22×10^{-21} cm^2, respectively for the $(^5S_2 + {}^5F_4) \rightarrow {}^5I_8$ transition of Ho^{3+} ions in YVO$_4$ phosphor. The values of $\sigma_p(\lambda)$ (3.22×10^{-21} cm^2) and β (0.816) for the green
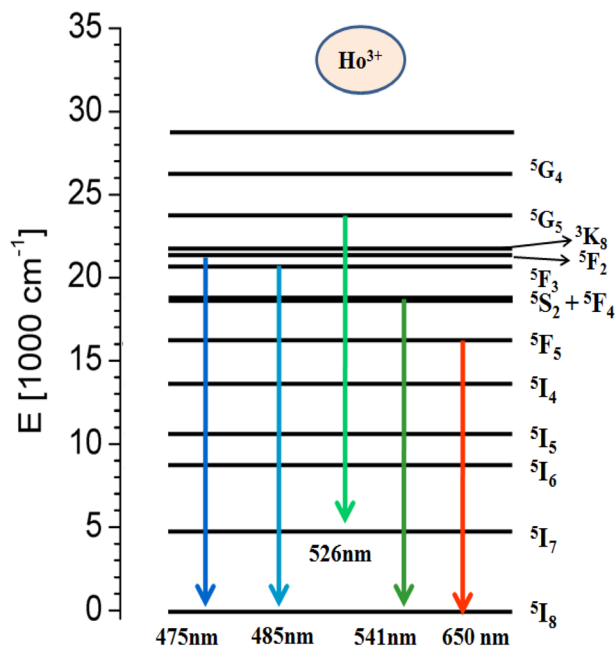
Fig. 8   Schematic energy level diagram of Ho^{3+} ion.
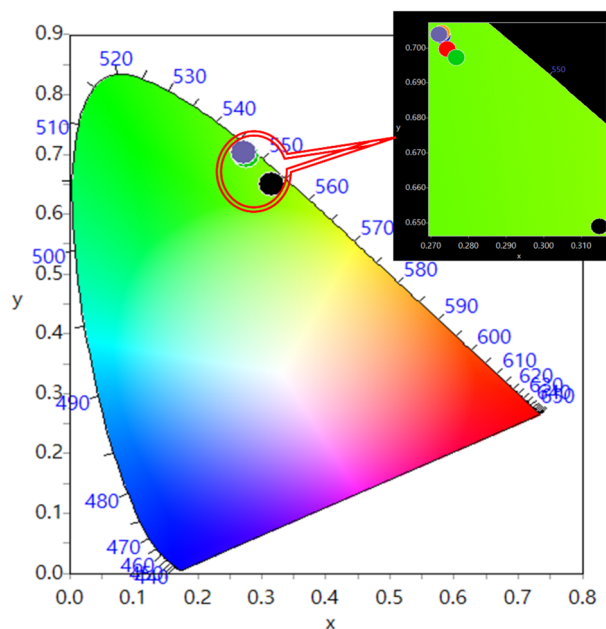
Fig. 10   CIE diagram for Y$_{1-x}$VO$_4$:xHo^{3+} phosphors.
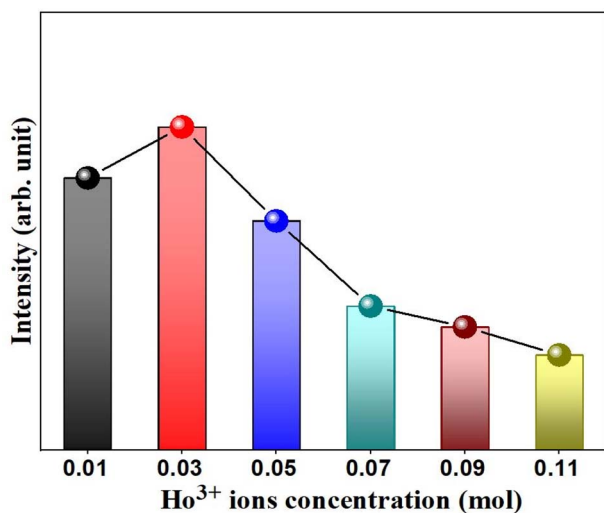
Fig. 9   Variation of emission intensity (I_{541nm}) as a function of Ho^{3+} concentration in the Y$_{1-x}$VO$_4$:xHo^{3+} phosphor.

Table 5   Commission International de l'Eclairage (CIE) color coordinates and color purity for the Y$_{1-x}$VO$_4$:xHo^{3+} phosphors using PL emission at λ$_{exc}$ = 310 nm

Y$_{1-x}$VO$_4$:xHo^{3+}	λ$_{exc}$ = 310 nm		
	x	y	Color purity (%)
x = 0.01	0.315	0.649	84.27(●)
x = 0.03	0.273	0.704	98.64(●)
x = 0.05	0.274	0.700	97.61(●)
x = 0.07	0.276	0.700	97.56(●)
x = 0.09	0.277	0.697	96.78(●)
x = 0.11	0.282	0.699	97.18(●)

emission of Ho^{3+}:YVO$_4$ are larger than Y$_2$O$_3$:Ho^{3+} (σ_p (λ) = 1.32 × 10^{-21} cm^2; β = 0.65),[58] which suggests that the Ho^{3+}:YVO$_4$ phosphor is a desirable optical material for low threshold and high gain applications. These remarkable results provide information on energy transfer from VO$_4^{3-}$ group to Ho^{3+} ions.

The CIE (Commission International de l'Eclairage) chromaticity coordinates of the prepared Y$_{1-x}$VO$_4$:xHo^{3+} phosphor materials are represented in Fig. 10. The results show that the CIE coordinates fall in the green region.[66,67] The color coordinates and color purity of the prepared phosphors are summarized in Table 5.

4.   Conclusions

In summary, we report herein the spectroscopic properties of a homogenous series of Y$_{1-x}$VO$_4$:xHo^{3+} phosphor materials synthesized using the sol–gel synthesis procedure. SEM analysis shows the irregular particles size of the phosphor. The preparation of a single-phase compound was confirmed by the XRD patterns. The optical transitions of Ho^{3+} ions are identified through diffuse reflectance spectrum. Using these absorption bands, the oscillator strength of the bands (f_{exp} & f_{cal}), the Judd–Ofelt parameters (Ω_λ, λ = 2, 4, & 6), total radiative transition probabilities (A_T), radiative lifetimes (τ_{rad}), and branching ratios (β) for the transition of Ho^{3+} ions in Y$_{0.97}$VO$_4$:0.03Ho^{3+} phosphor are reported. The energy conversion; and optical direct and indirect bandgaps are observed for YVO$_4$ phosphor doped with Ho^{3+} ions. In this approach, the energy transfer to the Ho^{3+} ions supports the results of the spectroscopic analyses. The phosphor exhibited a strong excitation band in the UV region at 310 nm while monitoring emission at 541 nm. Upon 310 nm

excitation, all the synthesized phosphors showed intense PL emission in the green region. Concentration quenching of Ho^{3+} ion was observed after 0.03 mol and this was mainly attributed to the electric multipolar interaction process. The $Y_{0.97}VO_4$:$0.03Ho^{3+}$ phosphor showed good emissive properties with very high color purity, suggesting that this material would be useful for green emitting devices.

Conflicts of interest

There are no conflicts to declare.

Acknowledgements

References

1 V. Panchal, S. Lopez-Moreno, D. Sanatamaria-Perez, D. Errandonea, F. J. Manjon, P. Rodriguez-Hernandez, A. Munoz, S. N. Achary and A. K. Tyagi, *Phys. Rev. B: Condens. Matter Mater. Phys.*, 2011, **84**, 02411.

2 V. Panchal, D. Errandonea, A. Segura, P. Rodrguez-Hernandez, A. Munoz, S. Lopez-Moreno and M. Bettinelli, *J. Appl. Phys.*, 2011, **110**, 43723.

3 N. Deligne, V. Gonze, D. Bayot and M. Devillers, *Eur. J. Inorg. Chem.*, 2008, **6**, 896–902.

4 E. V. Tsipis, V. V. Kharton, N. P. Vyshatko, A. L. Shaula and J. R. Frade, *J. Solid State Chem.*, 2003, **176**, 47–56.

5 Z. Xu, X. Kang, C. Li, Z. Hou, C. Zhang, D. Yang, G. Li and J. Lin, *Inorg. Chem.*, 2010, **49**, 6706.

6 Z. Y. Hou, P. P. Yang, C. X. Li, L. L. Wang, H. Z. Lian, Z. W. Quan and J. Lin, *Chem. Mater.*, 2008, **20**, 6686.

7 F. He, P. Yang, N. Niu, W. Wang, S. Gai, D. Wang and J. Lin, *J. Colloid Interface Sci.*, 2010, **343**, 71.

8 P. Huang, D. Chen and Y. Wang, *J. Alloys Compd.*, 2011, **509**, 3375.

9 L. Xie, H. Song, Y. Wang, W. Xu, X. Bai and B. Dong, *J. Phys. Chem. C*, 2010, **114**, 9975.

10 L. Li, M. Zhao, W. Tong, X. Guan, G. Li and L. Yang, *Nanotechnology*, 2010, **21**, 195601.

11 M. Yu, J. Lin and J. Fang, *Chem. Mater.*, 2005, **17**, 1783–1791.

12 A. Bao, H. Lai, Y. Yang, Z. Liu, C. Tao and H. Yang, *J. Nanopart. Res.*, 2010, **12**, 635–643.

13 E. A. Maunders and L. G. DeShazer, *J. Opt. Soc. Am.*, 1971, **61**, 684.

14 F. S. Ermeneux, R. Moncorge, P. Kabro, J. A. Capobianco, M. Bettinelli and E. Cavalli, *Adv. Solid State Lasers*, OSA, Washington, DC, 1996, p. SM9.

15 J. Sun, J. Zhu, X. Liu and H. Du, *Mater. Res. Bull.*, 2013, **48**, 2175–2179.

16 J. A. Coppabianco, P. Kabro, F. S. Ermeneux, R. Moncorge, M. Bettinelli and E. Cavalli, *Chem. Phys.*, 1197, **214**, 329–340.

17 M. Mahata, S. Tiwari, S. Mukherjee, K. Kumar and V. Rai, *J. Opt. Soc. Am. B*, 2014, **31**, 1814–1821.

18 J. E. Bernard and A. J. Alcock, *Opt. Lett.*, 1993, **18**, 968.

19 G. C. Bowkett, G. W. Baxter, D. J. Booth, T. Taira, H. Teranishi and T. Kobayashi, *Opt. Lett.*, 1194, **19**, 957.

20 D. Shen, A. Liu, J. Song and K. Ueda, *Appl. Opt.*, 1198, **37**, 7785.

21 X. Li, H. Xu, R. Yan, Y. Jiang, R. Fan, Z. Dong and D. Chen, *Optik*, 2021, **228**, 165789.

22 A. K. Levine and F. C. Palilla, *Appl. Phys. Lett.*, 1964, **5**, 118–120.

23 A. Bril, W. L. Wanmaker and J. Broos, *J. Chem. Phys.*, 1965, **43**, 311.

24 L. R. Singh and R. S. Ningthoujam, *J. Appl. Phys.*, 2010, **107**, 104304–104306.

25 W. M. Yen, S. Shionoya and H. Yamamoto, *Phosphor Handbook*, CRC Press, Boca-Raton, 2nd edn, 1999.

26 C. Hsu and R. C. Powell, *J. Lumin.*, 1975, **10**, 273–293.

27 M. Wu, S. Choi and H. K. Jung, *Mater. Res. Bull.*, 2016, **78**, 20–25.

28 U. Rambabu, D. P. Amalnerkar, B. B. Kale and S. Buddhudu, *Mater. Res. Bull.*, 2000, **35**, 929–936.

29 L. Shirmane, C. Feldmann and V. Pankratov, *Phys. B*, 2017, **504**, 80–85.

30 S. M. Rafiaei and M. Shokouhimehr, *Mater. Chem. Phys.*, 2019, **229**, 431–436.

31 K. E. Foka, B. F. Dejene and H. C. Swart, *Phys. B*, 2016, **480**, 95–99.

32 Y. Liu, H. Xiong, N. Zhang, Z. Leng, R. Li and S. Gan, *J. Alloys Compd.*, 2015, **653**, 126–134.

33 Z. Xu, X. Kang, C. Li, Z. Hou, C. Zhang, D. Yang, G. Li and J. Lin, *Inorg. Chem.*, 2010, **49**, 6706–6715.

34 X. Y. Huang, J. X. Wang, D. C. Yu, S. Ye, Q. Y. Zhang and X. W. Sun, *J. Appl. Phys.*, 2011, **109**, 113526.

35 V. A Medvedev, D. V. Mamonova, I. E. Kolesnikov, A. R. Khokhlova, M. D. Mikhailov and A. A. Manshina, *Inorg. Chem. Commun.*, 2020, **118**, 107990.

36 H. Zhou, W. Gao, P. Cai, B. Zhang and S. Li, *Solid State Sci.*, 2020, **104**, 106283.

37 Y. H. Li and G. Y. Hong, *J. Solid State Chem.*, 2005, **175**, 645–649.

38 S. Ekambaram and K. C. Patil, *J. Alloys Compd.*, 1995, **217**, 104–107.

39 A. Dwivedi, E. Rai, D. Kumar and S. B. Rai, *ACS Omega*, 2019, **4**, 6903–6913.

40 M. Yu, J. Lin, Z. Wang, J. Fu, S. Wang, H. J. Zhang and Y. C. Han, *Chem. Mater.*, 2002, **14**, 2224–2231.

41 L. D. Sun, Y. X. Zhang, J. Zhang, C. H. Yan, C. S. Liao and Y. Q. Lu, *Solid State Commun.*, 2002, **124**, 35–38.

42 G. Jia, Y. Song, M. Yang, Y. Huang, L. Zhang and H. You, *Opt. Mater.*, 2009, **31**, 1032–1037.

43 L. Zhu, J. Y. Li, Q. Li, X. D. Liu, J. Meng and X. Q. Cao, *Nanotechnology*, 2007, **18**, 055604–055609.

44 Y. H. Zhou and J. Lin, *Opt. Mater.*, 2005, **27**, 1426–1432.

45 M. R. Dolgos, A. M. Paraskos, M. W. Stoltzfus, S. C. Yarnell and P. M. Woodward, *J. Solid State Chem.*, 2009, **182**, 1964–1971.

46 W. O. Milligan and L. W. Vernon, *J. Phys. Chem. A*, 1952, **56**, 145–147.

47 Y. Sun, H. Liu, X. Wang, X. Kon and H. Zhang, *Chem. Mater.*, 2006, **18**, 2726–2732.

48 C. Shivakumara, R. Saraf and P. Halappa, *Dyes Pigm.*, 2016, **126**, 154–164.

49 B. R. Judd, *Phys. Rev.*, 1962, **127**, 750.

50 G. S. Ofelt, *J. Chem. Phys.*, 1962, **37**, 511.

51 A. A. Kaminskii, *Crystalline Lasers*, CRC Press, 1996.

52 W. T. Carnall, H. Crosswhite and H. M. Crosswhite, *Energy Level Structure and Transition Probabilities of the Trivalent Lanthanides in Laf*, Argonne National Laboratory, Argonne, IL, 1975.

53 M. Seshadri, E. F. Chillcce, J. D. Marconi, F. A. Sigoli, Y. C. Ratnakaram and L. C. Barbosa, *J. Non-Cryst. Solids*, 2014, **402**, 141.

54 Ş. Georgescu, A. Ştefan, O. Toma and A.-M. Voiculescu, *J. Lumin.*, 2015, **162**, 174–179.

55 M. Kaczkan and M. Malinowski, *Materials*, 2021, **14**, 3831.

56 M. Malinowski, Z. Frukacz, M. Szuflinska, A. Wnuk and M. Kaczkan, *J. Alloys Compd.*, 2000, **300–301**, 389–394.

57 M. Kaczkan, I. Pracka and M. Malinowski, *Opt. Mater.*, 2004, **25**, 345–352.

58 V. Singh, V. K. Rai, B. Voss, M. Haase, R. P. S. Chakradhar, D. T. Naidu and S. H. Kim, *Spectrochim. Acta, Part A*, 2013, **109**, 206–212.

59 B. M. Walsh, G. W. Grew and N. P. Barnes, *J. Phys.: Condens. Matter*, 2005, **17**, 7643–7665.

60 Q. Dong, G. Zhao, J. Chen, Y. Ding, B. Yao and Z. Yu, *Opt. Mater.*, 2010, **32**, 873–877.

61 S. R. Bullock, B. R. Reddy, P. Venkateswarlu and S. K. N. Stevenson, *J. Opt. Soc. Am. B*, 1197, **14**, 553–559.

62 A. Huignard, V. Buissette, A. Franville, T. Gacoin and J. Boilot, *J. Phys. Chem. B*, 2003, **107**, 6754–6759.

63 I. E. Kolesnikov, A. A. Kalinichev, M. A. Kurochkin, D. V. Mamonova, E. Y. Kolesnikov and E. Lahderanta, *J. Phys. Chem. C*, 2019, **123**, 5136–5143.

64 V. Singha, G. Lakshminarayana, A. Wagh and N. Singh, *Optik*, 2020, **207**, 164284.

65 G. Blasse, *Phys. Lett. A*, 1968, **28**, 444–445.

66 Monika, R. S. Yadav, A. Rai and S. B. Rai, *Sci. Rep.*, 2021, **11**, 4148.

67 P. Tadge, I. R. Martín, S. B. Rai, S. Sapra, T. M. Chen, V. Lavín, R. S. Yadav and S. Ray, *J. Lumin.*, 2022, **252**, 119261.